JOURNAL OF GUIDANCE, CONTROL, AND DYNAMICS
Vol. 18, No. 4, July–August 1995

Design and Examination of H_∞ Robust Controller for Ground Effect Problem

Kyoko Nitta*
Nagoya University, Aichi 464-01, Japan

An aeroelastic problem in the ground effect is treated. The H_∞ control theory based on the loop-shaping design procedure is applied to designing controllers for flutter suppression and attenuation of the aerodynamic disturbance caused by the ground irregulation. A two-dimensional flat-plate airfoil with three degrees of freedom, plunging, pitching, and control surface deflection is treated. The aeroelastic characteristics vary according to the altitude at which the airfoil is flying. Stability analysis and controller design are performed with the models with aerodynamic data obtained by the doublet-lattice method aerodynamic calculations and Padé approximation with two lag terms. Examination of robustness of the designed controllers are performed with numerical experiments using the finite difference method.

Nomenclature

A, A_c, A_d = state coefficient matrices
a = pitch axis location, referenced to midchord, in semichord
B, B_c, B_d = control coefficient matrices
b = semichord length
C, C_c, C_d, D_d = output coefficient matrices
c = hinge axis location, referenced to midchord, in semichord
C_L, C_M, C_N = aerodynamic coefficients of lift, moment about pitching axis, and control surface moment about hinge axis, respectively
Cl, Cm, Cn = nondimensional lift, moment about pitching axis, and control surface moment about hinge axis, respectively
G = control distribution vector
H = distance between airfoil and wall surface, in semichord
h = plunging degree of freedom, positive downward, in semichord
h_w = amplitude of wavy-wall surface, in semichord
K = generalized stiffness matrix
k = reduced frequency of oscillation based on semichord
k_h, k_α, k_β = uncoupled natural reduced frequencies based on semichord of plunging, pitching about elastic axis, and control surface deflection about hinge axis, respectively
k_w = reduced frequency of wavy-wall surface based on semichord
l = wavelength of wavy-wall surface, in semichord
M = generalized mass matrix
Q, Q_m = aerodynamic coefficient matrices
r_α, r_β = radii of gyration of airfoil about elastic axis and hinge axis, respectively
s = nondimensional Laplace operator, $s = ik$ for harmonic motion
t = time nondimensionalized by b/U
T_s = nondimensional sampling period
U = free-stream velocity
V = nondimensional velocity, $1/k_\alpha$
$W_1(s), W_2(s)$ = weighting functions in loop-shaping design procedure
x, y = orthogonal coordinates in semichord, or state and output vectors, respectively
z = nondimensional digital operator or augmented state vector
x_α, x_β = distances from elastic axis to mass center and hinge axis to control surface mass center, respectively, in semichords
α = angle of incidence, or pitching degree of freedom
β = control surface deflection degree of freedom
β_c = control surface command rotation
β_m = mth aerodynamic lag root
μ = airfoil–air mass ratio
ν = velocity ratio of wavy-wall surface
Ω = wave number of wavy-wall surface, in semichord

Received Sept. 25, 1993; revision received July 30, 1994; accepted for publication Feb. 26, 1995.

*Research Associate, Department of Mechanics and Aerospace Engineering.

Introduction

INCREASING demand of commuter transportation these days seems to activate the development of new types of vehicles. High-speed ground effect vehicles have become important for both passenger and cargo transportation, which can be located in the blank of the famous Gabrielli–von Kármán transportation efficiency chart. As for ordinary airplanes, the takeoff and landing phases are crucial in the flight envelope. Research on their flight conditions, that is, the flight conditions in proximity to the ground, is strongly required.

Many reports exist on the aerodynamic problem in the ground effect. A classical but enlightening way of research is the analytical approach,[1] for example, using conformal mapping.[2] A practical way to view this problem is shown in the comprehensive study by Pistolesi.[3] There also have been numerous researches that have adopted numerical approaches such as the vortex-lattice method. They cover the cases of steady and unsteady[4] or two-dimensional[5] and three-dimensional[6] problems. Many use the concept of a mirror image wing, which was first developed by Wieselsberger.[7] Recent application of this problem is to drag reduction by large eddy-breakup devices.[8]

Development of powerful computers allows researchers to solve the Navier–Stokes equation directly and simulate various situations concerned with wing-in ground (WIG) effects. More and more interesting results are obtained for application of WIG. In the road vehicle[9] and/or marine[10] industries, the ground effect problem is also studied earnestly. These studies certainly will aid in solving the ground effect problems.

However, the stability problem in ground effect does not seem to be fully inspected. A study concerned with stability analysis was performed by Kumar[11] classically. Using the matched asymptotic expansion method, Barrows et al. analyzed stability near the ground.[12] From the standpoint of control, maintaining safety in flight becomes

more difficult in proximity to the ground. The altitude may change rapidly, which causes an abrupt aerodynamic change. Moreover, in the vicinity of the ground, the flight condition rapidly changes because of obstacles such as bumps in the ground surface. In other words, there are a lot of uncertainties near the ground. Hence the importance of this problem can never be emphasized enough.

Today, active control technology (ACT) becomes a common design philosophy for stabilizing aeroelastic motion. There are numerous papers treating aeroelastic problems using ACT.[13–15] A common procedure to examine the control laws is wind tunnel testing. In order to examine the aerodynamic ground effect problem, experimental approaches have been performed in the past[16] and nowadays.[17] However, in order to simulate the ground, equipment such as moving belts or ground plates result in experiments that are large scale and expensive. Also the accuracy of simulation of the actual ground effect is always in question. Considering all of the above, numerical wind tunnel testing that includes the ground effect seems to be attractive for examination.

This paper is presented to suggest a way to apply ACT to the ground effect problem and to examine the robustness of the controller. Considering the uncertainties of the flight conditions, the control laws applied to the ground effect problem should be robust enough to ensure stability. The H_∞ control theory allows us to deal with a wide range of uncertainties. The loop-shaping design procedure (LSDP)[18] is adopted here because of its favorable aspects of the obtained controller. The examination of robustness of the obtained controllers are performed with numerical experiments using a finite difference method (FDM). In addition to the cases of the flat ground plane, disturbances caused by a moving wavy wall are considered. For the FDM computational scheme, the method of Ref. 19 is used with some modifications to implement the H_∞ controllers obtained with aerodynamic data calculated with the doublet-lattice method (DLM). The aerodynamic calculation part of the FDM code is a version of LTRAN2, which includes the higher order term with respect to time in the governing differential equation and boundary conditions and permits the maximum computable reduced frequency up to 0.8.[20] Using LTRAN2 and/or its versions, there are many reports treating the aeroelastic problem. Time response analysis is available with this kind of approach and was first carried out by Ballhaus and Goorjian.[21] For incompressible flows, there are more accurate methods to obtain aerodynamic models than the current approach based on the small perturbation potential equation. However, to quickly check the effectiveness of ACT, the current approach still seems very useful because of ease of programming and cost efficiency. Moreover, for flutter analyses in the transonic region, the small perturbation methods are still important tools.[22]

Problem Description

In this section, we will formulate the problem to be solved. The adopted control theory, i.e., the H_∞ control theory with the LSDP, is also explained briefly. The purpose of this paper is not to treat the control theory itself; hence the description is focused on the reason why this method is adopted. Interested readers should refer to the original lecture note.[18]

In order to construct a robust control law, in most cases designers are limited as to which control theory to adopt. The current paper treats the stabilization problem of a simple single-input, single-output (SISO) system. Hence we could adopt the classical, or linear quadratic Gaussian (LQG), control theory. However, if we adopt the classical design method, we have to be very careful with the stability, which is not known during the design procedure. If we adopt a modern control law such as the LQG, we have to work in the state space, which makes it difficult to define the weighting functions. When we solve a problem such as the H_∞ mixed-sensitivity problem, some of the obtainable closed-loop poles are located at the mirror image of unstable poles of the nominal model.[23] Hence for the design points at hand, some of the closed poles remain near the imaginary axis even after controlled, which give slow convergent characteristics to the closed-loop time history. The H_∞ control theory with the LSDP is adopted here for the following reasons. With this method, the weighting functions can be easily designed for high- and low-frequency regions by shaping the open-loop transfer function while

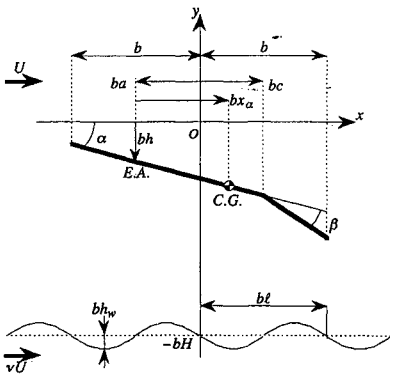

Fig. 1 Definition of parameters.

the closed-loop stability is assured. One of the advantages of this method is the ease in handling the poles on the imaginary axis and the availability of dealing with the change in the number of unstable poles. This situation is treated in the Results section.

System Modeling

For simplicity, a two-dimensional flat-plate airfoil in incompressible flow is treated. The airfoil is located in the free stream U in the x direction with three degrees of freedom (DOFs), plunging, pitching, and control surface deflection. No commuter aircraft flies very fast in proximity to the ground; therefore incompressibility would be an acceptable assumption. The ground surface is located just below the wing, with its vertical coordinate $-H$. Here, H is set to 5 (case 1) or 0.5 (case 2), which are the upper and lower limits where the ground effect problem can be meaningfully treated as a linear problem. Symbols and coordinates are illustrated in Fig. 1.

The governing equation of the vertical motion of the airfoil is given as

$$M\ddot{x} + Kx = p + G\beta_c \tag{1}$$

where

$$x = [h \quad \alpha \quad \beta]^T$$

$$G = \begin{bmatrix} 0 & 0 & r_\beta^2 k_\beta^2 \end{bmatrix}^T$$

$$M = \begin{bmatrix} 1 & x_\alpha & x_\beta \\ x_\alpha & r_\alpha^2 & (c-a)x_\beta + r_\beta^2 \\ x_\beta & (c-a)x_\beta + r_\beta^2 & r_\beta^2 \end{bmatrix}$$

$$K = \begin{bmatrix} k_h^2 & 0 & 0 \\ 0 & r_\alpha^2 k_\alpha^2 & 0 \\ 0 & 0 & r_\beta^2 k_\beta^2 \end{bmatrix}$$

The overdots denote differentiation with time t normalized by b/U. All the values except t are nondimensionalized by semichord length b. The structural damping term is neglected. In order to obtain a constant coefficient matrix, state space, aeroelastic model, the aerodynamic load vector p is expressed as

$$p = \frac{1}{\pi\mu}[-Cl \quad Cm \quad Cn]^T = \frac{1}{\pi\mu}Qx \tag{2}$$

where

$$Q = \begin{bmatrix} -C_{Lh} & -C_{L\alpha} & -C_{L\beta} \\ 2C_{Mh} & 2C_{M\alpha} & 2C_{M\beta} \\ 2C_{Nh} & 2C_{N\alpha} & 2C_{N\beta} \end{bmatrix}$$

In the aerodynamic calculation, to obtain the nominal model, the DLM with a mirror-image wing is used. To express the result in the complex s plane, the Padé approximation

$$Q = Q_0 + Q_1 s + Q_2 s^2 + \sum_{m=1}^{N} \frac{Q_{m+2} s}{s + \beta_m} \tag{3}$$

is adopted. This approximation has been widely used in the design of active flutter suppression systems. The aerodynamic coefficients are calculated for simple harmonic motion of several values of k and approximated in the above form. The aerodynamic lag terms β_m are arbitrarily selected for the range of reduced frequencies from the DLM calculation. The matrices Q_0 through Q_{N+2} are chosen so as to give the best least squares fit to Q over a range of reduced frequencies.

The resultant equations to be solved are expressed as

$$\left(M - \frac{1}{\pi\mu}Q_2\right)\ddot{x} - \frac{1}{\pi\mu}Q_1\dot{x} + \left(K - \frac{1}{\pi\mu}Q_0\right)x - \frac{1}{\pi\mu}\sum_{m=1}^{N} x_{Am} = G\beta_c$$
$$\dot{x}_{Am} = Q_{m+2}\dot{x} - \beta_m x_{Am} \tag{4}$$

When we use the state vector z including the displacements, their derivatives, and augmented aerodynamic state variables and express the control surface command rotation β_c as the input vector u, we can get the familiar expression of the state equation. Adding the output equation, the equations to be solved are

$$\dot{z} = Az + Bu \qquad y = Cz \tag{5}$$

Throughout this paper, the output signal y is selected to be the airfoil plunging motion h.

Controller Design and Calculation Procedure

Here we will give a quick overview of the controller design procedure. At first, the plant is augmented with weighting functions so as to achieve the desired specifications. The H_∞ controller is then obtained in the class of stabilizing controllers. Finally, the weighting functions are coupled with the obtained controller in order to get the final controller.

The resultant controller is expressed in the state space form

$$\dot{z}_c = A_c z_c + B_c y \qquad u = C_c z_c \tag{6}$$

The bilinear transformation

$$s = \frac{2}{T_s}\frac{1 - z^{-1}}{1 + z^{-1}} \tag{7}$$

has been used in order to implement the digital version of the obtained controllers. Then the control dynamics calculation is performed with the difference equations

$$z_d(n+1) = A_d z_d(n) + B_d y(n)$$
$$u(n) = C_d z_d(n) + D_d y(n) \tag{8}$$

Numerical Experiment Procedure

A FDM is adopted to examine the designed control laws. For the FDM aerodynamic calculation, the method of Ref. 19 is used. In order to implement the designed controllers, some modifications are added. The algorithm is shown in Fig. 2 in block diagram form. The parameters Cl, Cm, and Cn are calculated in the aerodynamic subroutine with the boundary condition using h, α, β, and their derivatives obtained in the previous time step. Equation (5) is a set of differential equations to be solved step by step following the change of the flow field immediately after the aerodynamic calculation in order to get the new values of h, α, β, and their derivatives. The time step sizes used in aerodynamic and structural dynamics calculations are the same.

For the continuous controllers, the control dynamics calculation is performed using Eq. (6) at each step immediately after the aerodynamic and structural dynamics calculation. For this case, the time step for the aerodynamic and structural dynamics calculation is also used for the control dynamics calculation. For the digitized controllers, the control dynamics calculation is performed using Eq. (8) at each sampling time using the output information at that time.

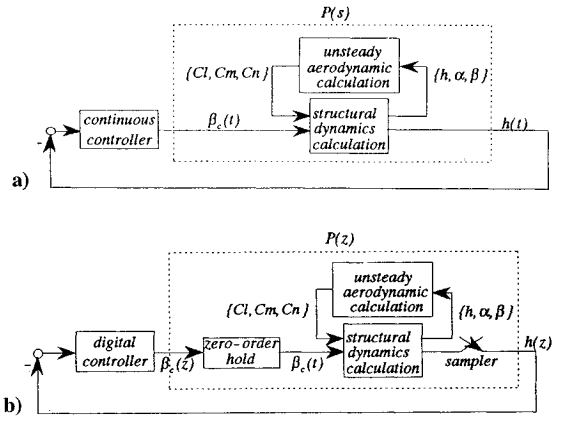

Fig. 2 Block diagram of FDM calculation: a) with continuous controller and b) with digitized controller.

Results

In this section, models used in designing controllers are called DLM models as they use DLM calculation results for aerodynamic augmented states. The models obtained by FDM aerodynamic calculations are called FDM models. The aeroelastic parameters of the airfoil are[13]

$$k_h/k_\alpha = 0.5 \qquad k_\beta/k_\alpha = 3.0 \qquad \mu = 40.0$$
$$a = -0.4 \qquad c = 0.6 \qquad x_\alpha = 0.2$$
$$r_\alpha^2 = 0.25 \qquad x_\beta = 0.0125 \qquad r_\beta^2 = 0.00625$$

Examination of DLM Models

Prior to searching for efficient control laws, the aeroelastic characteristics of the nominal models should be examined. In order to reduce the size of the nominal models, N in Eq. (3) is taken as 2 whereas most others use four aerodynamic lag terms.[14] The harmonic motions relating the three modes were calculated using values of k from 0.0 to 1.0 in increments of 0.1. Considering the range of calculated reduced frequencies, the values of β_m were selected as 0.05 and 0.5 at first. The curve fit seemed to be quite reasonable. With these values, when nondimensional velocity V increased, in case 2 the torsion branch went into the right-half plane (RHP) whereas in case 1 the bending branch became the flutter mode. However, the bending mode became unstable in both cases when four lag terms were used (0.2, 0.4, 0.6, 0.8 or 0.05, 0.15, 0.3, 0.5). The eigenvalue root loci seriously differ according to the number and the values of the aerodynamic poles. Although the root pair 0.5 and 0.05 was not used this time, the fact that the torsion branch only went into the RHP in case 2 suggests an interesting aspect of the aeroelastic characteristics according to height: The torsional component of the flutter mode is more predominant in case 2 than in case 1.

In order to rearrange the lag roots that can closely approximate the behavior of the actual systems, the results of $H = \infty$ (case 0) were compared with the exact root loci using Bessel functions.[13] In this calculation, the DLM without a mirror-image wing was used. Jones's approximation, whose lag roots are 0.0455 and 0.3, gives almost the same root loci for case 0 as the exact solution. This pair was also tried but showed poorer agreement when used in Eq. (3) because of the higher order terms in the interpolation function. Finally, the lag terms are rearranged as $\beta_m = 0.05, 0.25$, which gave the closest root loci in all the examined pairs of lag roots. In Ref. 15, it is stated that the best selection of the lag pole is the open-loop flutter frequency if a single lag term is used. The frequency 0.25 is almost the flutter frequency for both cases 1 and 2. The flutter velocities V_F, which are the velocities when the bending branch goes into the RHP, are 3.0102, 2.9488, and 2.4681 for cases 0, 1, and 2, respectively. Nearer the ground, larger aerodynamic forces make the flutter velocity significantly lower.

Choosing appropriate design points is very important to obtain favorable closed-loop characteristics. This time, $V = 3.0$ for case 1 and $V = 2.5$ for case 2 are selected. We choose these design points

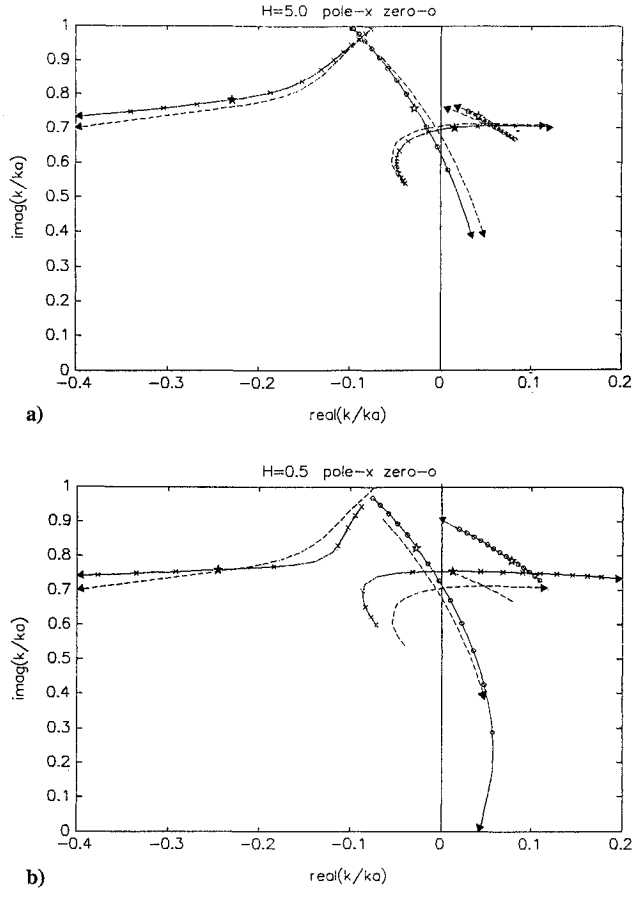

Fig. 3 Pole–zero examination of DLM models: a) case 1 and b) case 2.

(the eigenvalue due to the bending mode is almost on the imaginary axis but in the RHP) because our purpose is to suppress flutter using ACT. The concept is that no aircraft can fly at speeds much higher than the flutter speed, namely deep in the RHP.

The aerodynamic characteristics change drastically as a function of height in the ground effect region. Coincidentally, the aeroelastic characteristics change, although the structural parameters of the airfoil remain the same. In order to examine the above-mentioned phenomena more generally, it is convenient to look at the pole–zero location of the models. The pole–zero plots are calculated by parametrically changing the nondimensional velocity V up from $V = 2.0$ to $V = 3.5$ (Fig. 3). The plots represent all 0.5 values of V. The stars are for the pole–zero locations of the design points. The broken lines are pole–zero plots of case 0 for comparison. It is shown that, in both cases, at least one zero is in the RHP. Especially for case 1, pole–zero locations are very close to each other around $V = 3.1$. For that case, the flutter mode becomes almost uncontrollable. The ground effect is favorable considering pole–zero cancellation is avoided. Moreover, the RHP zero locates farther from the origin in case 2 than in case 1, which would make the largest achievable bandwidth higher below which effective disturbance attenuation is possible. Hence from the standpoint of achieving performance, case 2 is favorable compared with case 1.

It is interesting to see the behavior of cases 1 and 2 in comparison with case 0. In case 2, torsion and bending branches coalesce so tightly in the subcritical region that they almost unite. Moreover, compared with case 1, they separate each other much more rapidly. It means that once an unstable motion occurs, the increase of instability of case 2 is much harder than cases 0 and 1. Case 1 behaves similar to case 0, but the two branches do not coalesce as much.

The flutter conditions for both cases were also examined with the time histories of DLM models (results not shown). In case 2, where V_F is much lower than case 1, the amplitude of the bending displacement was smaller. However, the torsion and control surface displacement were almost the same. Again we can see the difference of the predominant modes.

Numerical Experiment Results

At first, examination of the FDM models was performed. The results are simply explained here without figures because of the space limitation. For case 1, the FDM flutter velocity is 3.1 whereas in the DLMs it is 2.9488. For case 2, the FDM flutter velocity is 2.6 whereas in the DLMs it is 2.4681. It suggests the unstable poles of the design point of DLM models are still in the left-half plane in FDM models for both cases. In the physical situation, some damping must exist, which would make the degree of instability smaller compared with DLM models. Remember that DLM models do not include even the structural damping in Eq. (1). Hence FDM models can be treated as the real systems with damping, and the procedure taken for the ordinary wind tunnel testing is performed. Fast Fourier transform (FFT) was performed using the time history data of impulse responses of FDM models and compared with the Bode plots of DLM models. The critical peak near the natural frequencies of bending and torsion seemed to be modeled well, whereas the roll-off characteristics were different in the high-frequency region. Numerical errors in the FFT calculation may be the most possible reason, because the same procedure was performed with DLM models and the same phenomenon was observed. Another possible reason is, of course, the modeling error.

The uncertainties in the FDM models are attributed to differences in aerodynamic forces and calculations of structural integration. With respect to these two parameters closer examinations of the FDM models were performed.

The former is examined in Ref. 19 by comparison of the pressure distribution on the airfoil. They were in good agreement, however; the FDM values were lower at the leading edge of the airfoil and the control surface. It causes the aerodynamic force to be less in the FDM models than in the DLM models. In order to certify the aerodynamic calculation of FDM and get more information near the ground, another examination was performed by solving Euler and Navier–Stokes equations and comparing the pressure contours of the flow field. They agreed very well in spite of the fact that the governing equations are different.

In order to examine the latter, i.e., structural integration, two techniques were tested in the FDM calculation. In Ref. 24, some integrators are suggested and compared. The transient matrix method seemed excellent and was applied to the comparison with the Runge–Kutta procedure, which is currently used in the FDM for integration of the structural dynamics equation.[19] The integrators presented almost the same time histories for every case examined. The Runge–Kutta method seems to treat the dynamic motion of the airfoil more directly, so the Runge–Kutta integration method is adopted in the numerical integration of both the structural and control dynamics calculations. The time step for aerodynamic and structural dynamics calculation is 360 per cycle of the bending mode.

Controller Design

Figure 4 shows the Bode plots of the nominal DLM models. Because the design points are very near the critical flutter conditions, the first peaks are almost at the flutter frequencies for both cases. We can ascertain that the contribution of the torsion mode is greater in case 2 from the peak locations. The second peaks are the control surface mode. We can use this information directly in the LSDP. The poles are very close to the zeros, which makes designing the weighting function difficult. After some trial and error, the designed weighting function is the same for both models and has the notch filter form

$$W_1(s) = \frac{0.05\left(s^2 + 2k_\alpha s + 16k_\alpha^2\right)}{s^2 + 0.7k_\alpha s + 0.49k_\alpha^2} \tag{9}$$

This is designed to alleviate the flutter mode with appropriate input cost.

Initial Value Responses with and Without Control

Next, initial value responses are examined including control. The FDM calculations are performed following the procedure given in Fig. 2a. The DLM models include unstable poles, which make the initial value [$h(0) = 0.01$ and all the other variables are zero] responses of the nominal models diverge. Although the aerodynamic

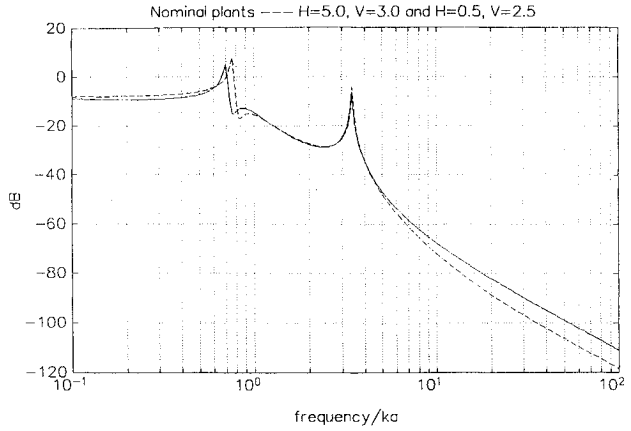

Fig. 4 Comparison of Bode plots; case 1, solid line; case 2, broken line.

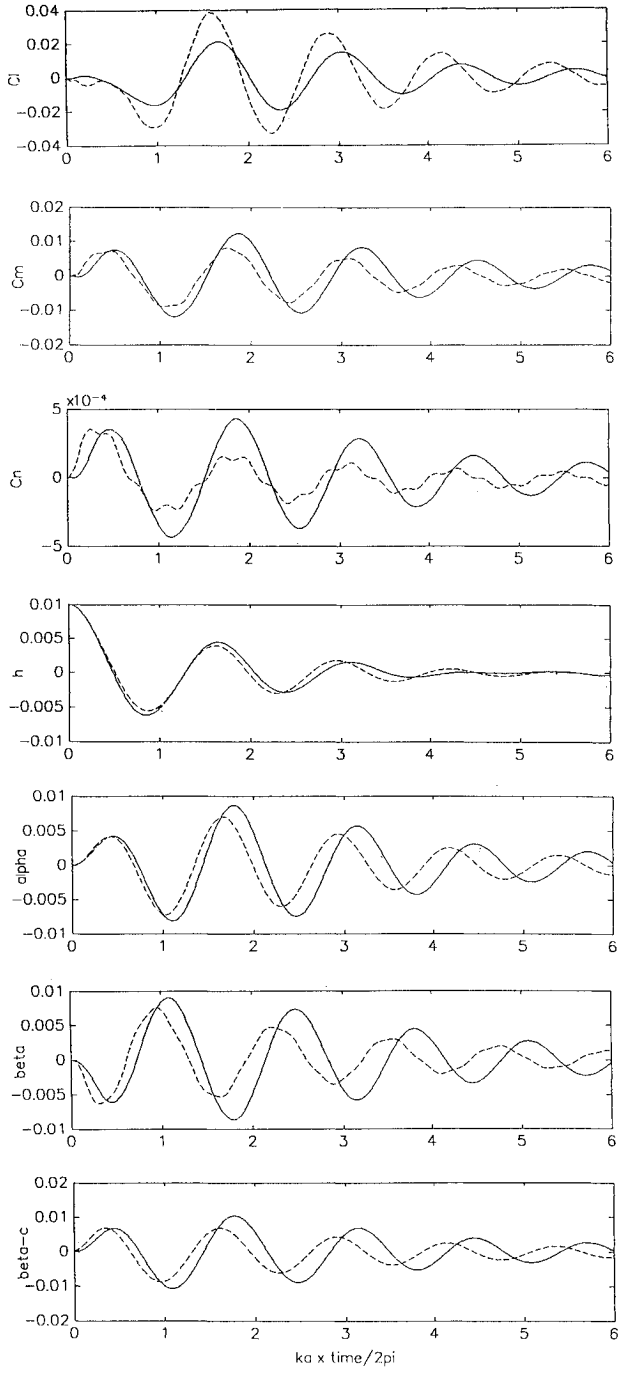

Fig. 5 Initial value response of FDM models with continuous W_1 controllers: case 1, solid line; case 2, broken line.

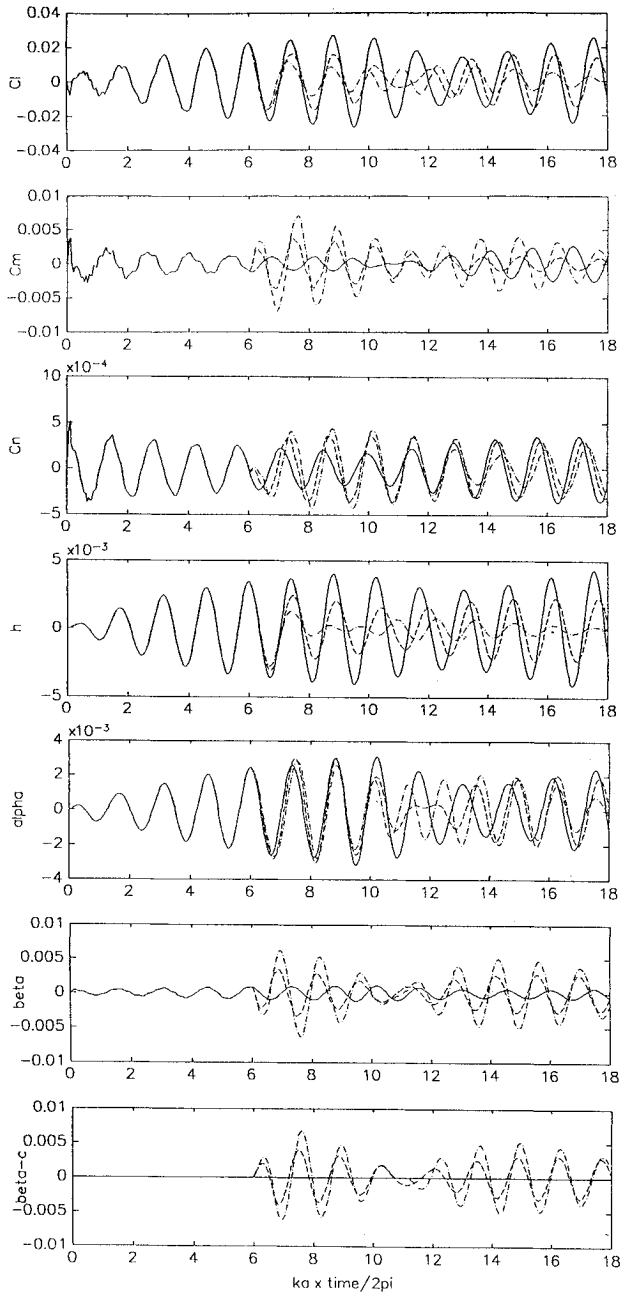

Fig. 6 Time history of case 2 over wavy-wall surface (l = 1): without control, solid line; with continuous W_1 controller, broken line; with continuous W_2 controller, dot-dashed line.

forces are greater in case 2 because of the ground effect, displacements are smaller because the unstable pole of the design point is slightly shallower in the RHP in case 2 than in case 1 (see Fig. 3). On the other hand, the FDM models do not include unstable poles. Hence the time histories converge. However, bending poles are very near the imaginary axis. It is just the situation where the control is required to avoid getting unstable. The amplitudes of the displacements are almost the same between cases 1 and 2, which tells us that the critical root of case 1 is closer to the imaginary axis. The phase lags are almost the same between DLM and FDM models.

Figure 5 shows the time histories of the controlled FDM models. Because the weighting function in designing controllers is the same [Eq. (9)] for cases 1 and 2, the time histories of the controlled variable h are similar to each other. It is interesting to see that although the airloads are greater in case 2, the required input cost is greater in case 1. It may come from the pole–zero location. In case 1, DLM pole–zero locations are close to each other in the RHP. We can expect that in FDM models it is again true because DLM models approximate FDM models well, as examined above.

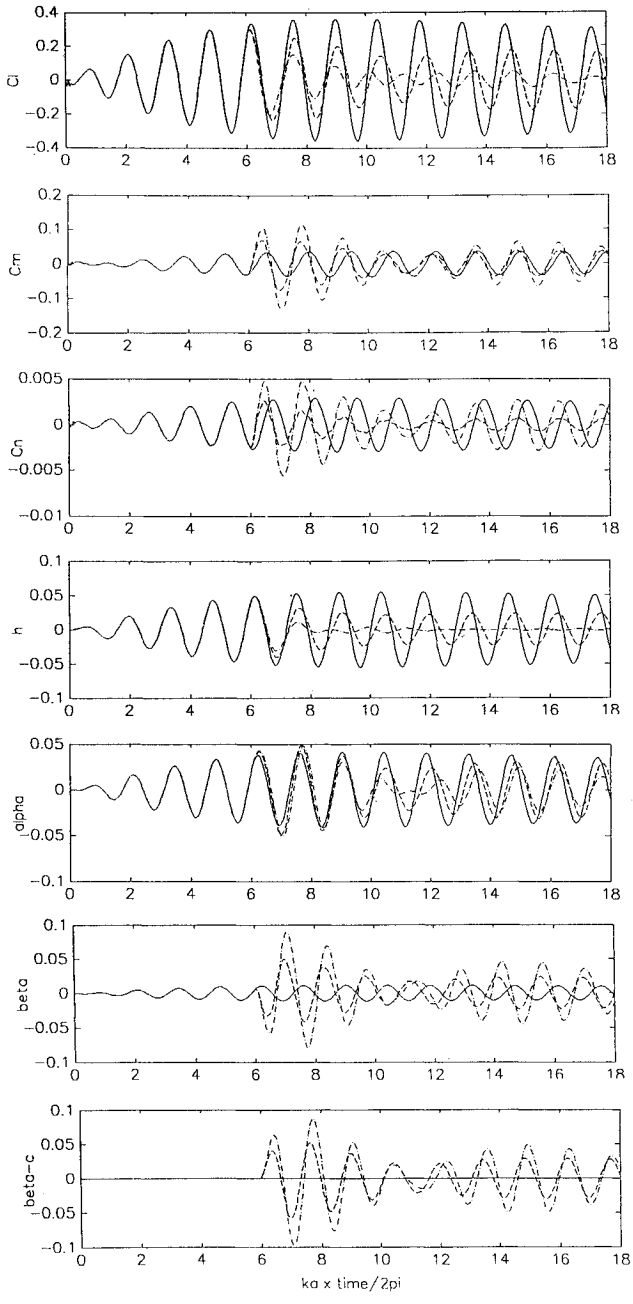

Fig. 7 Time history of case 2 over wavy-wall surface (l = 5): without control, solid line; with continuous W_1 controller, broken line; with continuous W_2 controller, dot-dashed line.

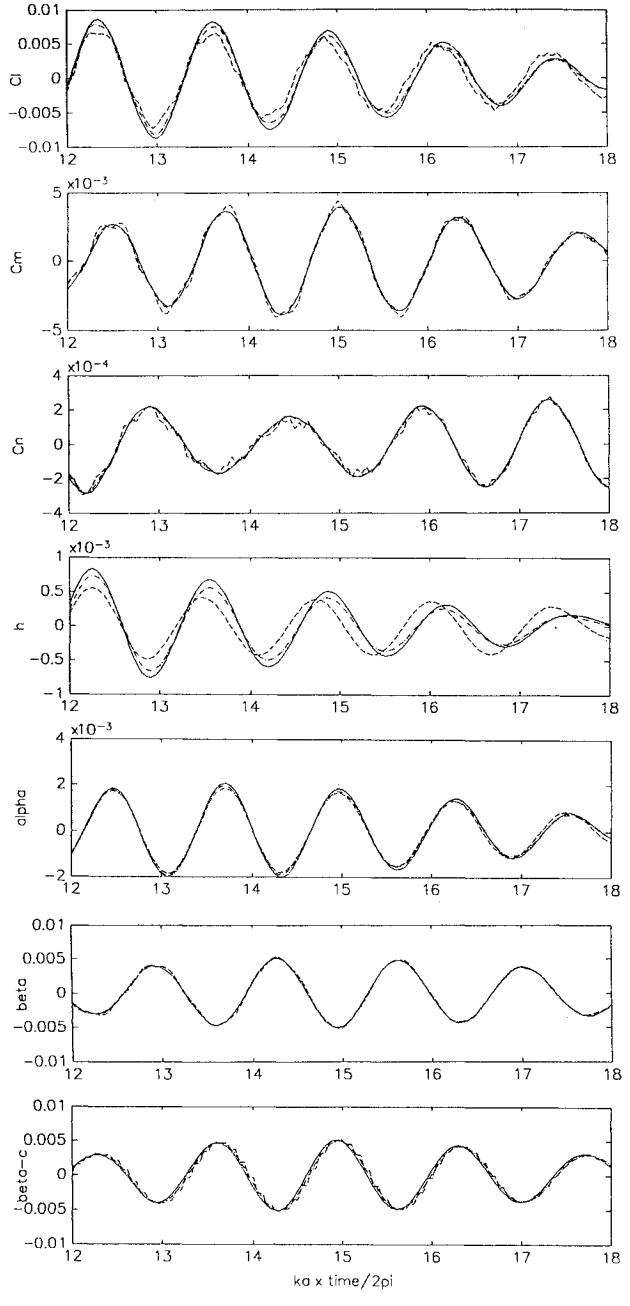

Fig. 8 Last part of time history calculation of case 2 over wavy-wall surface with W_2 controller (l = 1): continuous, solid line; digitalized with $k_s = 20k_\alpha$, dot-dashed line; digitalized with $k_s = 10k_\alpha$, broken line.

Wavy-Wall Disturbance

From here on, only case 2 is dealt with. A moving wavy wall is introduced to the system. Under the airfoil, an infinite wavy-wall surface travels with the velocity vU whose mean line lies on $y = -H$ and the wave amplitude is h_w (see Fig. 1). For simplicity, the wall surface is assumed to keep harmonic motion. The vertical displacement and velocity of the wall surface are then expressed as

$$\begin{aligned} y &= -H + h_w \sin[k_w(t - x/v)] \\ w_w &= h_w(k_w - \Omega)\cos(k_w t - \Omega x) \end{aligned} \tag{10}$$

where we assume $h_w \ll l$ (small disturbance). The reduced frequency of the wall, k_w, is defined as $k_w \equiv 2\pi v/l$, where l is the wavelength of the wavy-wall surface. Here, $\Omega \equiv 2\pi/l$ is the wave number of the wavy wall. In the current calculation, the fixed parameters of the wavy wall are $h_w = 0.01$ and $k_w = 0.7k_\alpha$, which seems to be the most severe situation because it is almost the flutter frequency.

The time histories without control are shown in Figs. 6 (l = 1) and 7 (l = 5) as solid lines. It is interesting to note that the responses differ a lot for different wavelengths even though the frequency of coming wavy wall is the same. The difference of Ω in Eq. (10) causes the transient responses of the time histories to differ considerably. The phenomena of this transient part can be explained as the resonance of the wave frequency and the natural frequencies of the airfoil.

After the free motion of first six cycles of the torsion mode, the controllers with W_1 are tested (Figs. 6 and 7, broken lines). Compared with the responses without control, the amplitudes are reduced but the oscillations still remain.

The internal model theorem is adopted here to obtain a more efficient control law for this case. The modified weighting function is

$$W_2(s) = \frac{0.025\left(s^2 + 2k_\alpha s + 16k_\alpha^2\right)}{s^2 + 0.49k_\alpha^2} \tag{11}$$

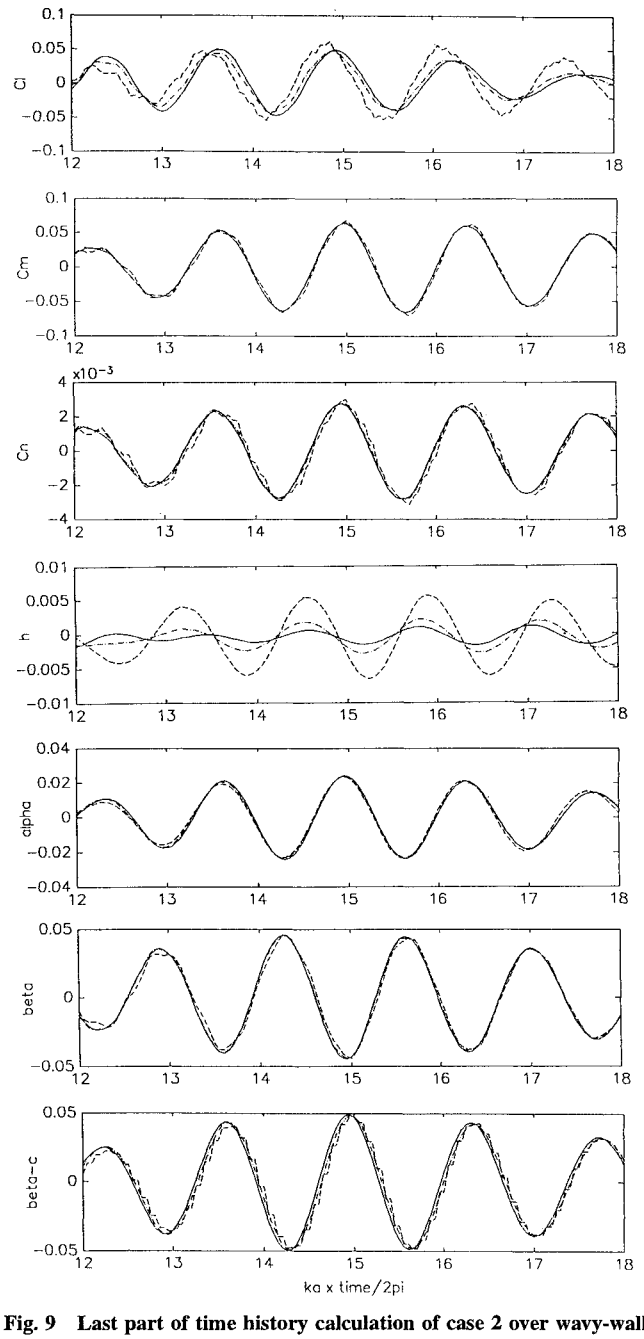

Fig. 9 Last part of time history calculation of case 2 over wavy-wall surface with W_2 controller ($l = 5$): continuous, solid line; digitalized with $k_s = 20k_\alpha$, dot-dashed line; digitalized with $k_s = 10k_\alpha$, broken line.

which gives the specified pole at the wall frequency to the obtained controller. Although there exist uncertainties, FDM models can be controlled efficiently with this controller (Figs. 6 and 7, dot-dashed lines). As the output signal is h, the amplitudes of h are reduced for both cases whereas α and β are not. Especially, the amplitudes of β are increased because of the input cost.

Treatment of Implementation of Controllers

In order to simulate the real wind tunnel testing, the controllers obtained in the continuous region are discretized using Eq. (7). The FDM model can be treated as a discrete system with a sampler and a zero-order holder, as already described in Fig. 2b. The control dynamics calculation procedure for this case follows Eq. (8) whereas structural integral equations remain the same. The results of implementation of the digitalized W_2 controllers with the disturbance of the wavy wall are shown in Figs. 8 and 9, which show the last six cycles of the torsion mode in the calculations. The sampling frequencies are taken to be $k_s = 20k_\alpha$ (dot-dashed lines) and $k_s = 10k_\alpha$ (broken lines). Solid lines are with the continuous controller. Considering the wall frequency, $k_s \cong 14k_\alpha$ would be the "safe" sample rate.[25] For wavelength $l = 1$, there seems to be little deterioration with digitalization even for $k_s = 10k_\alpha$. However, for the case $l = 5$, the output signal h with $k_s = 10k_\alpha$ oscillates much harder than the other two cases although its amplitude is decreased compared with the nominal oscillation. For cases 1 and 2, almost no deterioration was observed in the initial value response with the digitalized W_1 controllers. With this method, one can have a quick view of deterioration caused by discretization of controllers.

Conclusions

The ground effect stability problem has been studied. To summarize:

1) The characteristics of the three-DOF airfoil at different altitudes are examined. The aeroelastic nature differs between $H = 5$ and $H = 0.5$, which affects controllability of plants. The contribution of the torsion mode to instability is greater when the airfoil is closer to the ground.

2) The stability problem is solved with the H_∞ control theory using the loop-shaping design procedure.

3) Numerical experiments using a FDM are performed. Under the uncertainties of modeling errors and wavy-wall disturbances, perturbed models are efficiently controlled, which ensures the robustness of the obtained controllers.

Acknowledgments

The author acknowledges Hirobumi Ohta for his continuous support of this research. Thanks are also due to the reviewers and editors of this paper.

References

[1]Plotkin, A., and Dodbele, S. S., "Slender Wing in Ground Effect," *AIAA Journal*, Vol. 26, No. 4, 1988, pp. 493, 494.

[2]Tomotika, S., Nagamiya, T., and Takenouti, Y., "The Lift on a Flat Plate Placed Near a Plane Wall, with Special Reference to the Effect of the Ground upon the Lift of a Monoplane Aerofoil," Rept. of the Aeronautical Research Inst., Tokyo Imperial Univ., Vol. 8, No. 97, 1933.

[3]Pistolesi, E., "Ground Effect—Theory and Practice," NACA TM-828, 1937.

[4]Nuhait, A. O., and Mook, D. T., "Numerical Simulation of Wings in Steady and Unsteady Ground Effects," *Journal of Aircraft*, Vol. 26, 1989, pp. 1081–1089.

[5]Bagley, J. A., "The Pressure Distribution on Two-Dimensional Wings Near the Ground," Aeronautical Research Council 3238, London, 1961.

[6]Katz, J., "Calculation of the Aerodynamic Forces on Automotive Lifting Surfaces," *Journal of Fluids Engineering*, Vol. 107, 1985, pp. 438–443.

[7]Wieselsberger, C., "Wing Resistance Near the Ground," NACA TM-77, 1922.

[8]Dowing, A. P., "The Effect of Large-Eddy Breakup Devices on the Oncoming Vorticity," *Journal of Fluid Mechanics*, Vol. 160, 1985, pp. 447–465.

[9]Hashiguchi, M., Ohta, T., and Kuwahara, K., "Computational Study of Aerodynamic Behavior of a Car Configuration," AIAA Paper 87-1386, 1987.

[10]Kohara, S., and Nakato, M., "Numerical Computation on Surface Waves Generated by a Running Pressure Disturbance," *Journal of the Society of Naval Architects of Japan*, Vol. 171, 1992, pp. 41–52.

[11]Kumar, P. E., "Stability of Ground Effect Wings," CoA. Rept. AERO No. 196, May 1967.

[12]Barrows, T. M., Widnall, S. E., and Richardson, H. H., "The Use of Aerodynamic Lift for Application to High Speed Ground Transportation," Office of High Speed Ground Transportation, FRA-RT-71-56, 1970.

[13]Edwards, J. W., Breakwell, J. V., and Bryson, A. E., Jr., "Active Flutter Control Using Generalized Unsteady Aerodynamic Theory," *Journal of Guidance and Control*, Vol. 1, No. 1, 1978.

[14]Abel, I., "An Analytical Technique for Predicting the Characteristics of a Flexible Wing Equipped with an Active Flutter-Suppression System and Comparison with Wind-Tunnel Data," NASA TP 1367, 1979.

[15]Nissim, E., "Reduction of Aerodynamic Augmented States in Active Flutter Suppression Systems," *Journal of Aircraft*, Vol. 18, No. 1, 1991, pp. 82–93.

[16]Reid, E. G., "A Full Scale Investigation of Ground Effect," NACA TR 265, 1927.

[17]Chawla, M. D., Edwards, L. C., and Franke, M. E., "Wind-Tunnel Investigation of Wing-in-Ground Effects," *Journal of Aircraft*, Vol. 27, 1990, pp. 289–293.

[18]McFarlane, D. C., and Glover, K., "Robust Controller Design Using Normalized Coprime Factor Plant Descriptions," Lecture Notes in Control and Information Sciences, 138, Springer–Verlag, Berlin, 1990.

[19]Nitta, K., "Analysis of Aerodynamics of Airfoils Moving over a Wavy Wall," *Journal of Aircraft*, Vol. 31, 1994, pp. 387–395.

[20]Nakamichi, J., "An Improved Version of the LTRAN2 for High Frequency Domain," *Transactions of the Japan Society for Aeronautical and Space Sciences*, Vol. 27, No. 77, 1984, pp. 121–133.

[21]Ballhaus, W. P., and Goorjian, P. M., "Computation of Unsteady Transonic Flows by the Indicial Method," *AIAA Journal*, Vol. 16, 1978, pp. 117–124.

[22]Crouse, G. L., Jr., and Leishman, J. G., "Transonic Aeroelasticity Analysis Using State Space Unsteady Aerodynamic Modeling," *Journal of Aircraft*, Vol. 29, No. 1, pp. 153–160.

[23]Sefton, J., and Glover, K., "Pole/Zero Cancellations in the General H_∞ Problem with Reference to a Two Block Design," *Systems and Control Letters*, Vol. 14, 1990, pp. 295–306.

[24]Edwards, J. W., Bennet, R. M., Whitlow, W., and Seidal, D. A., "Time-Marching Transonic Flutter Solutions Including Angle-of-Attack Effects," *Proceedings of the AIAA/ASME/ASCE/AHS 23rd Structures, Structural Dynamics, and Materials Conference* (New Orleans, LA), Pt. 2, AIAA, New York, 1982, pp. 220–233.

[25]Franklin, G. F., Powell, J. D., and Emami-Naeini, A., *Feedback Control of Dynamic Systems*, Addison–Wesley, Reading, MA, 1986.